



# **Simulation of Wireless Fading Channels**

Ronnie Gustafsson  
Abbas Mohammed

Department of Telecommunications and Signal Processing  
Blekinge Institute of Technology

# Simulation of Wireless Fading Channels

R. Gustafsson, A. Mohammed

Department of Telecommunications and Signal Processing  
Blekinge Institute of Technology  
Ronneby, Sweden

May 2003

## Abstract

Future services in wireless communications will increase the need for high bit rates in the system because of the use of “wideband” contents such as streaming video and audio. For example, there might be services where the users can download movies to the car theatre system, or where a user can react to the doorbell ringing even though he or she is miles away from home. It will be possible to run business software remotely using mobile devices, removing the need for “dumb down” software in the terminal devices. Also, users might want to be able to seamlessly roam between different air interfaces or standards using the same device. Some basic services are already implemented in the existing 2G systems such as GSM or IS-136, more services are planned for the new 3G systems and other advanced features have to wait until 2011 when 4G is scheduled for release. The demands for higher bit rates combined with the ever-increasing number of users, however, introduces the need for clever and efficient usage of the limited resource of the wireless channel.

Two major impediments to high-performance wireless communication systems are intersymbol interference (ISI) and cochannel interference (CCI). ISI is caused by the frequency selectivity (time dispersion) of the channel due to multipath propagation and CCI is due to cellular frequency reuse. Equalizers can be used to compensate for ISI and CCI can be reduced by the use of adaptive antenna arrays (also known as “smart antennas”). The smart antenna utilizes an array of antenna elements that provide directional (spatial) information about the received signals. Since the desired signal and unwanted cochannel interferers generally arrive from different directions, an adaptive beamforming algorithm can adjust the spatial gain to enhance the desired signal and mitigate the cochannel interferers.

In this Report we discuss the basic propagation mechanisms affecting the performance of wireless communication systems. We also present the implementation of a simulator which takes these mechanisms into account and verifies its performance for different channels. We also introduce basic equalization and beamforming concepts. Finally, we evaluate the recursive least squares (RLS) equalizer and receiver structures and assess their performance in combating the destructive effects of the channel.

# Contents

<b>1</b>	<b>Introduction</b>	<b>2</b>
1.1	The wireless channel . . . . .	2
1.2	Adaptive Equalization Techniques . . . . .	7
1.3	Adaptive Beamforming Techniques . . . . .	10
<b>2</b>	<b>Simulation assumptions and system model</b>	<b>11</b>
2.1	Functional blocks of the simulator . . . . .	11
2.2	Continuous vs. slotted transmission . . . . .	13
2.3	Representation of signals . . . . .	14
2.4	Modulation techniques . . . . .	14
2.4.1	Binary phase shift keying . . . . .	14
2.4.2	Quaternary phase shift keying . . . . .	15
2.4.3	$\pi/4$ -differential quaternary phase shift keying . . . . .	15
2.5	The square-root raised cosine filter (pulse shaping) . . . . .	16
2.6	Channel model . . . . .	18
2.6.1	Simulation of the fading channel coefficient . . . . .	19
2.6.2	Construction of the discrete time impulse response . . . . .	19
2.6.3	The spatial-temporal channel model . . . . .	20
<b>3</b>	<b>Computer experiments</b>	<b>22</b>
3.1	Design of the discrete time impulse responses . . . . .	22
3.2	Simulation of a system with AWGN . . . . .	25
3.3	Simulation of a time-invariant channel . . . . .	25
3.4	Simulation of a Rayleigh fading channel . . . . .	25
3.5	Simulation of a frequency selective fading channel . . . . .	28
3.6	Simulation of a RLS equalizer for a frequency selective fading channel . . . . .	34
3.7	Simulation of a RLS beamformer for a frequency selective fading channel . . . . .	37
<b>4</b>	<b>Conclusions</b>	<b>39</b>

# Chapter 1

## Introduction

A typical *uplink* scenario is shown in Figure 1.1, where a transmitter (such as a mobile phone) broadcasts a signal containing digital information, such as encoded speech or data, intended for the base station to receive. Due to imperfections of the wireless channel *noise*, *intersymbol interference* and *cochannel interference* are introduced, which causes errors in the transmission and degrades the quality of wireless communications. We can use adaptive *equalization techniques* to combat the intersymbol interference and adaptive *beamforming schemes* (see Figure 1.2) to mitigate the effects of cochannel interference. Consequently, these techniques can significantly improve the capacity and quality of wireless networks.

In this Chapter, we discuss the *fading* phenomena in wireless communication channels and briefly present the equalizer and beamformer structures. The channel simulator that we have developed and implemented is presented in Chapter 2. In Chapter 3 we verify the simulator in terms of bit error rate for typical scenarios as well as evaluating the performance of RLS based equalizer and beamformer structures. Finally Chapter 4 concludes this Report.

### 1.1 The wireless channel

The propagation factors that affect the strength of the received signals in wireless communication systems, excellently introduced in [Chr02], are the *path loss*, *large-scale fading* and *small-scale fading*. These are explained briefly below:

- The path loss is basically a drop in signal power as a function of distance. When a mobile receiver moves away from the base station, i.e. when the distance increases, the signal will become weaker because of

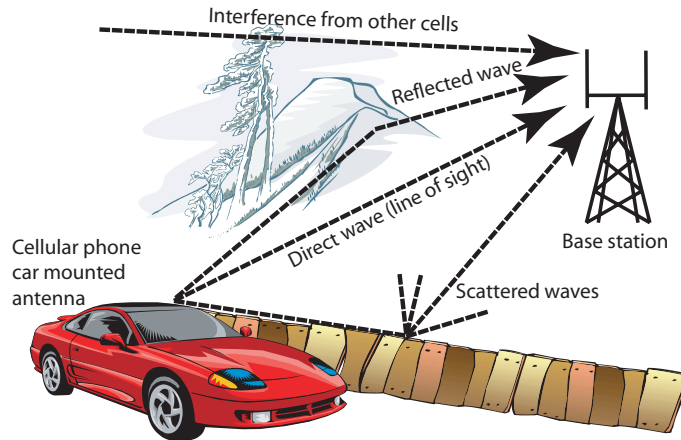


Figure 1.1: *A typical uplink scenario. The user transmits a signal which reaches the base station via line of sight or by reflection and scattering. Signals from other users in other cells introduce cochannel interference at the base station.*

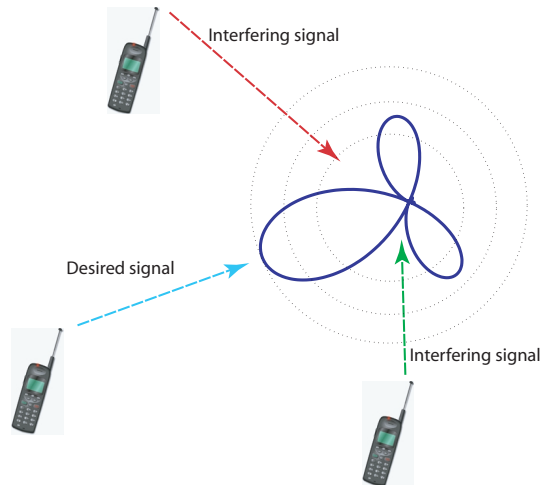


Figure 1.2: *A beamformer in operation, where a lobe (beam) is formed/directed towards the desired user and the interfering users are nulled out.*

power loss in the transmission medium. For free-space propagation, the signal strength is inversely proportional to the distance squared (i.e.,  $1/d^2$ , where  $d$  is the distance between the transmitter and receiver). Measurement of wireless channels have found out that, in practice, the signal strength decreases more rapidly than  $1/d^2$ ; a typical value often used in predicting propagation of wireless channels is  $1/d^4$ . The path loss has the lowest rate of change of the three factors and the attenuation normally reaches 100-120 dB in the coverage area.

- The large-scale fading varies faster than path loss and is normally described as a log-normal distributed stochastic process around the mean of path loss. This type of fading is introduced because of the shadowing from buildings and other structures in the environment. The large-scale fading introduces attenuations of about 6-10 dB.
- The small-scale fading is, as the name implies, the fastest varying mechanism. It is introduced as a consequence of the multipath propagation together with the time-varying nature of the channel. The small-scale fading attenuates the signal with up to 40 dB when the mobile moves as short as half a wavelength.

The path loss and large-scale fading can be mitigated by the use of power control, for example. Small-scale fading, on the other hand, introduces the need of an equalizer that is capable of removing the time-varying intersymbol interference introduced by the multipath propagation.

The multipath propagation arises from the fact that the transmitted signal is *reflected* from objects such as buildings or mountains, *scattered* from smaller objects such as lamp posts and *diffracted* at edges of houses and roof-tops [Sta02] for example. Hence, the signal will reach the receiver from different directions, as shown in Figure 1.1. Each path may have different delay, introducing a spread in time (Delay spread) of the received signals, indicating that the channel may be characterized by an impulse response, where each impulse represents signal path with a certain delay. Depending on the maximum difference in time between the first and last received signals, the *maximum excess delay*  $T_m$ , and the rate at which the symbols are transmitted, the *symbol rate*  $T_s$ , the channel may be classified as *frequency selective* or *flat*. The channel is said to be frequency selective when  $T_m > T_s$ , because different frequencies of the transmitted signal will experience different amount of attenuation. On the other hand, if  $T_s < T_m$  then the channel is said to be flat since all frequencies of the transmitted signal would experience essentially the same amount of attenuation.

For wireless systems, the channel is time-variant because of the relative motion between the transmitter and the receiver or by movements of objects within the channel, which results in propagation changes (i.e., variations in the signal's amplitude and phase).

Another important physical mechanism that affects the signal is the *Doppler effect*. For example, if the transmitter is fixed and the receiver is moving relatively to it, a transmitted sinusoid in a single-path case will be shifted (i.e. up or down-modulated) because of the Doppler shift. Thus, in a multipath environment, the total effect on the received signal will be seen as a Doppler spreading or spectral broadening of the transmitted signal frequency.

If we assume that (i) the propagation of the waves takes place in the two-dimensional (horizontal) plane, (ii) that there is isotropic scattering around the receiver, (iii) that the channel is flat, (iv) uniform distribution of signals arriving from all angles throughout the range  $[0, 2\pi]$  and that (v) the receiving antenna is omni directional, then it is possible to show that, when there is a great number of waves received at the antenna, a transmitted signal will be multiplied with a time-varying signal with a power spectral density in literature often called *Jake's power spectral density*, *Clarke's power spectral density* or *the classical Doppler spectrum*, see Figure 1.3. Interested readers are referred to [Cla68] for full details regarding the derivation of Jake's PSD.

It can also be shown that the signal has a complex Gaussian distribution, which implies that the magnitude of the signal will have a *Rayleigh distribution*, in the case of no line-of-sight, see Figure 1.4. When a line-of-sight component is present, the distribution will be *Rician* instead. A nice presentation on this topic can be found in [Pt02]. In Figure 1.5 we have plotted one realization of a Rayleigh fading signal which has the classical Doppler spectrum.

Combining the fact that the channel introduces multipath fading, i.e. that the channel may be characterized by an impulse response (assuming the channel to be linear), and that the signal is scattered around the receiver, the final model of the channel is a time-varying impulse response, where each coefficient in the response models a certain multipath; i.e. each coefficient will have the classical Doppler spectrum and either a Rayleigh or Rician distribution. Note that apart from the Rician case, the received signal can not be said to come from any specific direction (i.e., the impinging waves have no specific angle-of-arrival). For the Rayleigh and Rician processes, it is possible to derive a number of useful statistical properties [Pt02, NH01], such as the *average fade duration (AFD)*, the *level crossing rate (LCR)*, and the *autocorrelation function*.

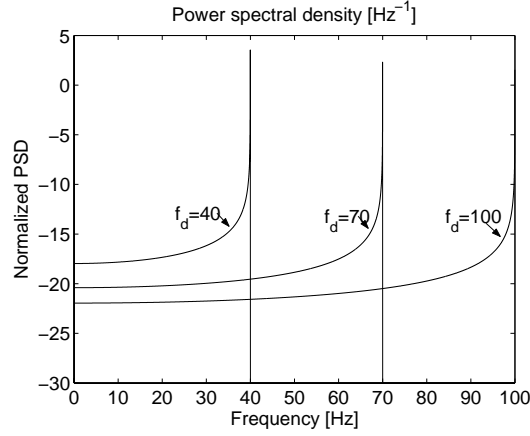


Figure 1.3: *The normalized power spectral density for a Rayleigh fading channel for different Doppler frequencies  $f_d$ . This PSD is denoted as the classical Doppler spectrum.*

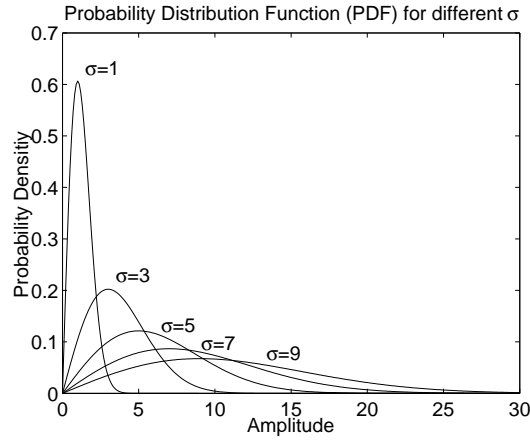


Figure 1.4: *The probability density function for a Rayleigh fading signal for different values of the standard deviation  $\sigma$  of the underlying complex Gaussian process.*

The AFD is a measure of the average time the amplitude of the signal is below a certain threshold level. In Figure 1.6 the AFD is shown for different values of the Doppler frequency, where it is clearly shown that the higher the Doppler frequency, the shorter the fades will be on the average.

The LCR is a measure of how often a certain amplitude level is passed by the signal as shown in Figure 1.7. It is clear from this Figure that for a higher Doppler frequency, the rate of crossing for a certain level is higher.

The autocorrelation function which is shown in Figure 1.8 specifies the extent to which there is correlation between the channel's impulse response at time  $t_1$  and at time  $t_2$ . It can be seen that for higher Doppler frequencies, the time dependence goes down (i.e., less correlation).

An excellent overview on this topic and other channel modelling techniques is presented in [ECS<sup>+</sup>98].

## 1.2 Adaptive Equalization Techniques

If the duration of the impulse response of the channel (i.e. the *delay spread*) is sufficiently large, there will be intersymbol interference in which parts of the signal leaks out and interferes with the next symbols in the transmission, resulting in errors in the received data sequence. An equalizer may be used to cancel the effects of the channel, with the goal that the combined effect of the wireless channel and the equalizer equals an impulse response of a delayed unit impulse, which means perfect equalization. The equalizer has to be fast enough to be able to adapt the equalizer weights as the channel impulse response varies with time. The faster channel variations (or *fades*), the faster equalizer is needed.

There are several types of equalizers with different properties that may be used to equalize the channel [Sma94, Hoo94, Pro95, Tid99]. The most straight forward equalizer is the *linear equalizer*, where a filter in serial with the channel is adapted so that it becomes the channel inverse (inverse filtering). Algorithms such as the *least mean squares (LMS)* or the *recursive least squares (RLS)* may be used to adapt the filter, where the error signal that drives the filter coefficients is found as the difference between the filter output and a desired training signal (a *pilot signal* or *training sequence*).

A drawback with the linear equalizer is the requirement of a training sequence. The transmission of such a signal occupies bandwidth that may otherwise be used for the user data. An alternative which avoids this problem is to use *blind equalization techniques*, such as the so called Busgang equalizer [Hay02], which doesn't require the use of training sequences. In its most general form, the equalizer consists of a linear transversal filter followed

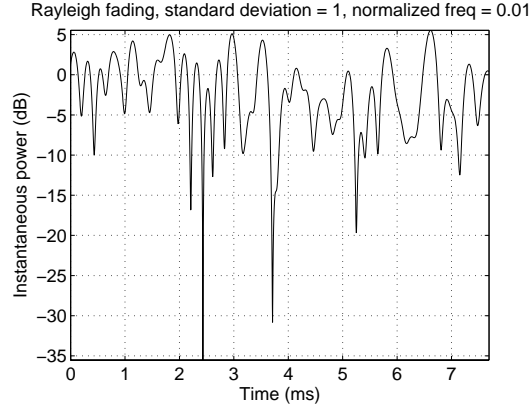


Figure 1.5: *A realization of a Rayleigh fading signal with a classical Doppler spectrum.*

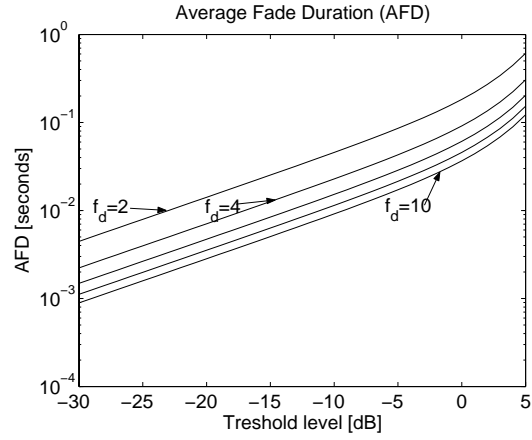


Figure 1.6: *The average fade duration for different values of the Doppler frequency  $f_d$ .*

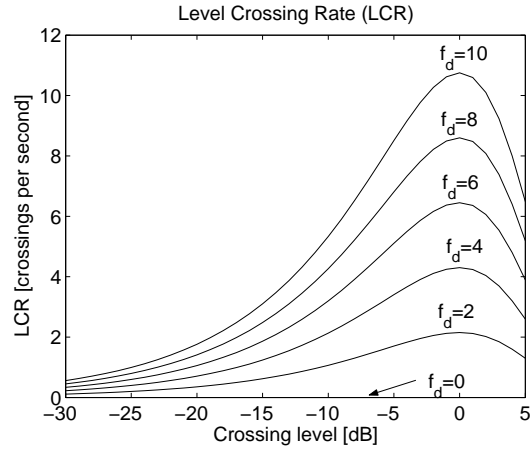


Figure 1.7: *The level crossing rate for different values of the Doppler frequency  $f_d$ .*

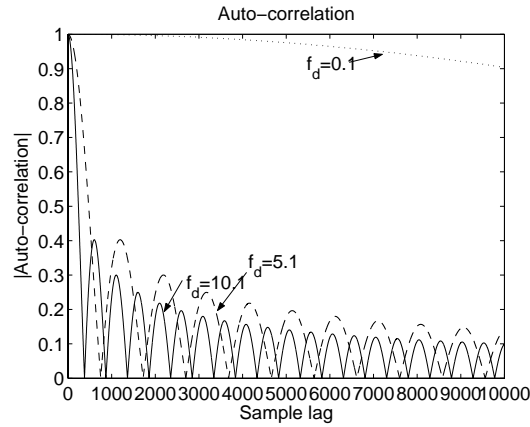


Figure 1.8: *The autocorrelation for different values of the Doppler frequency  $f_d$ .*

by a non-linearity. The idea is to subtract the output of the non-linearity from its input in order to construct an error signal that can drive the filter coefficients, instead of using a training sequence as in the linear equalizer. A suboptimal implementation of the equalizer may be derived, where the choice of non-linearity is the hyperbolic-tangent function with an adjustable slope by the so called *slope-parameter*. The slope of the non-linearity is gradually increased by an annealing controller, in order to speed up the convergence. There are several special cases of the Bussgang equalizer, for example the *Sato* and *Godard* equalizers. A special case of Godard is the *constant modulus algorithm (CMA)*, which differ from the Bussgang in the choice of the non-linearity. An interesting feature of CMA is that it decouples the issue of removing the ISI and adjusting the phase of the signal; the CMA may be followed by a *phased locked loop (PLL)* that takes care of the phase changes in the signal constellation.

The objective of both the non-blind linear transversal equalizers and the blind Bussgang equalizers is the same: to find the inverse filter of the channel. One way to increase the performance of the equalizer is to use *decision feedback*, where the decisions from the equalizer are fed back through a *feedback filter*, in order to subtract the ISI from former symbols. The impulse response of the channel can be said to consist of *precursor* ISI, a reference coefficient and *postcursor* ISI [Tid99, Sma94]. The job of the *feedforward filter* is to remove the precursor ISI and keep the reference coefficient at unity; the postcursor ISI is removed by the feedback filter.

## 1.3 Adaptive Beamforming Techniques

A beamformer may be used to form lobes in the directions of the signals of interest and place nulls in the directions of unwanted signals (the cochannel interferers), as shown in Figure 1.2. To be able to do this, we need to use multiple antennas at the receiver; specifically  $K$  antennas in a linear array are able to null  $K - 1$  interfering signals. In Chapter 4, we use a linear array in order to investigate the performance of a RLS based *spatial-temporal beamformer*. The simulator is capable of simulating circular arrays, but we do not investigate the performance of such arrays in this Report.

## Chapter 2

# Simulation assumptions and system model

In order to make it possible to develop and implement the equalization and beamforming receiver structures for wireless communications, we have to be able to evaluate their performance in realistic environments. The most realistic scenario is of course to implement these structures in hardware and to evaluate their performance in real-time with real signals. However this approach would be too expensive and time-consuming in this early stage of the process. Another appealing approach is to record the data received by the antennas and then evaluate it off-line. In this Report, we have chosen the cheapest and least time-consuming approach; that is to implement a *simulator* that still gives us realistic environments and an indication about the performance of the different algorithms. The simulator is schematically shown in Figure 2.1.

### 2.1 Functional blocks of the simulator

The simulator shown in Figure 2.1 consists of 15 processing blocks that implements the various aspects of a typical wireless communications system. Each block has its own functionality which is described below:

The first block (**block 1**) generates the *binary* data that will be transmitted over the system. The data can consist of continuous symbols or it can be formatted slots which contains for example training sequences. We denote the first type of data sequence as *unslotted data* and the second type as *slotted data*. Our simulator is capable of generating both types of data, where the slotted data is formatted in a similar way as the one used in IS-54 standard.

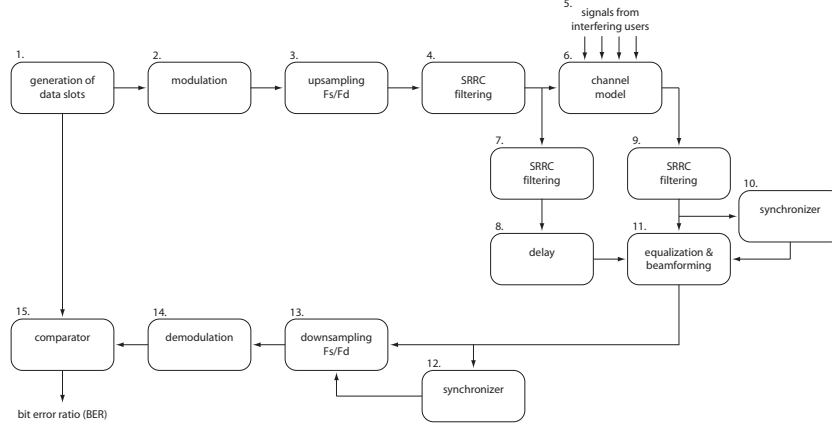


Figure 2.1: *Overview of the simulator that has been implemented and used in all simulations.*

The modulator (**block 2**) is responsible of modulating the binary data with the chosen modulation technique. The simulator supports binary phase shift keying (BPSK), quaternary phase shift keying (QPSK) and  $\pi/4$  differential phase shift keying ( $\pi/4$ -DQPSK). The output from the block is, in general, a sequence of symbols (i.e. complex numbers) at the symbol rate  $F_d$  symbols/second.

The interpolator (**block 3**) increases the sampling frequency to the frequency used in the system,  $F_s$  samples/second, by inserting  $F_s/F_d - 1$  zeros between each input sample. The output is a sequence of “zero-padded” symbols. The fraction  $F_s/F_d$  is denoted the *over sampling factor*, and set to either 1 or 13 in the simulations described in Chapter 3.

In order to limit the bandwidth used by the transmitter, the pulse train from the interpolator is filtered or shaped (*pulse shaping*) by filters (**block 4, 7 and 9**) in a way that does not introduce intersymbol interference. In our simulator we use square-root raised cosine (SRRC) filters at both the transmitter and receiver sides. The combination of the filters at both sides fulfils the Nyquist criteria.

A total of  $P - 1$  interfering users may be added in the channel by using  $P - 1$  extra instances of blocks 1 to 4 (**block 5**) to produce interfering signals.

The channel model or simulator (**block 6**) implements both time-invariant and time-variant channel impulse responses. Both frequency selective fading and flat fading may be generated for different velocities. The Rayleigh fading signals are generated by Jakes method [Jak94, NH01, DHFM02].

The transmitted signal is filtered by a second SRRC filter (**block 7**) and delayed (**block 8**) in order to produce a desired signal that may or may not

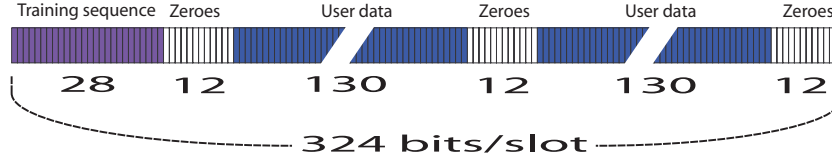


Figure 2.2: *Slot format used in the simulator. Each slot begins with a 28 bit training sequence followed by 12 zeros, 130 user data bits, 12 zeros, 130 data bits and finally 12 zeros ending the slot.*

be used by the equalizer (**block 11**). The delay is used to relax the demands on the equalizer.

After the receiver SRRC filter (**block 9**) the equalizer or beamformer (**block 11**) tries to remove the interference from the signal. The equalizer may use the synchronization signal produced by the synchronizer (**block 10**), but this is optional.

After equalization, a synchronizer (**block 12**) finds the optimal sampling point, which is used by the sampler (**block 13**) to produce a signal at the symbol rate.

The symbol rate signal is then demodulated (**block 14**) and compared to the transmitted data in the comparator (**block 15**) in order to calculate the bit error rate in the system.

## 2.2 Continuous vs. slotted transmission

As mentioned above, the simulated transceiver operates in either *continuous* or *slotted* mode. In continuous mode the data sequence to be transmitted is completely unformatted, containing uncorrelated random symbols only. In slotted mode, on the other hand, the sequence is formatted.

The format used for the slotted mode is shown in Figure 2.2. It is a similar format as the one used in IS-54 standard on the downlink [CHLP94]; each slot begins with a 28 bit training sequence followed by 12 zeros, 130 user data bits, 12 zeros, 130 data bits and finally 12 zeros ending the slot. This adds up to a total of 324 bits per slot or 162 symbols if each symbol represents two bits, as in QPSK modulation, for example.

It is only the desired user that may transmit slotted data; all interfering users adding up to the cochannel interference are modelled in continuous mode.

The 28-bit training sequence used by the desired user contains the bits:

$$1\ 0\ 1\ 0\ 1\ 0\ 0\ 1\ 0\ 0\ 0\ 1\ 1\ 1\ 0\ 1\ 1\ 1\ 1\ 0\ 0\ 1\ 0\ 0\ 1\ 0\ 1\ 0 \quad (2.1)$$

It is also denoted the *synchronization word*, since it may be used for synchronization purposes.

## 2.3 Representation of signals

Any signal  $x(t)$  in a real system implementation, i.e. a continuous time real-valued signal, with a frequency content concentrated in a narrow band of frequencies near the carrier frequency  $f_c$ , can generally be written as [Chr02]

$$x(t) = a(t) \cos(2\pi f_c t + \theta(t)) \quad (2.2)$$

This expression can be rewritten as

$$\begin{aligned} x(t) &= a(t) \cos[2\pi f_c t + \theta(t)] \\ &= \operatorname{Re} \{a(t) \exp(j\theta(t)) \exp(j2\pi f_c t)\} \\ &\quad \operatorname{Re} \{\tilde{x}(t) \exp(j2\pi f_c t)\} \end{aligned} \quad (2.3)$$

where we have defined

$$\tilde{x}(t) = a(t) \exp(j\theta(t)) \quad (2.4)$$

We call the signal  $\tilde{x}(t)$  the *complex envelope* or *complex baseband* representation of the signal  $x(t)$ , since it has its frequency content centered around DC.

All signals that we work with in the simulator are baseband, since baseband signals may be sampled by a lower sampling rate than the original non-baseband signals.

## 2.4 Modulation techniques

### 2.4.1 Binary phase shift keying

Binary phase shift keying (BPSK) is the simplest of the modulation methods. In BPSK the constellation diagram contains only two message points, as shown in Figure 2.3. Let  $m(n)$  contain the sequence of ones and zeros to be transmitted, then the constellation points may be calculated by the formula:

$$y(n) = e^{j\pi m(n)} \quad (2.5)$$

We see that

$$\begin{aligned} m(n) = 0 &\Rightarrow y(n) = e^{j\pi \cdot 0} = e^0 \Rightarrow \angle y(n) = 0 = 0^\circ \\ m(n) = 1 &\Rightarrow y(n) = e^{j\pi \cdot 1} = e^{j\pi} \Rightarrow \angle y(n) = \pi = 180^\circ \end{aligned} \quad (2.6)$$

i.e.  $y(n)$  takes values of the expected constellation points.

### 2.4.2 Quaternary phase shift keying

The constellation diagram for quaternary phase shift keying (QPSK) is shown in Figure 2.4. If  $m(n)$  contains a sequence of data from the set  $[0, 1, 2, 3]$ , representing the symbols that we want to transmit: 00, 01, 11, and 10 respectively then the constellation points may be calculated by the formula:

$$y(n) = e^{j\frac{\pi}{4} + j\pi m(n)/2} \quad (2.7)$$

We see that

$$\begin{aligned} m(n) = 0 &\Rightarrow y(n) = e^{j\frac{\pi}{4} + j\pi \cdot 0/2} = e^{j\frac{\pi}{4}} \Rightarrow \angle y(n) = \frac{\pi}{4} = 45^\circ \\ m(n) = 1 &\Rightarrow y(n) = e^{j\frac{\pi}{4} + j\pi \cdot 1/2} = e^{j\frac{3\pi}{4}} \Rightarrow \angle y(n) = \frac{3\pi}{4} = 135^\circ \\ m(n) = 2 &\Rightarrow y(n) = e^{j\frac{\pi}{4} + j\pi \cdot 2/2} = e^{j\frac{5\pi}{4}} \Rightarrow \angle y(n) = \frac{5\pi}{4} = 225^\circ \\ m(n) = 3 &\Rightarrow y(n) = e^{j\frac{\pi}{4} + j\pi \cdot 3/2} = e^{j\frac{7\pi}{4}} \Rightarrow \angle y(n) = \frac{7\pi}{4} = 315^\circ \end{aligned} \quad (2.8)$$

i.e.  $y(n)$  takes values of the expected constellation points.

### 2.4.3 $\pi/4$ -differential quaternary phase shift keying

In  $\pi/4$ -differential QPSK ( $\pi/4$ -DQPSK) the information is carried in the phase shifts of the transmitted signals, rather than in the phase itself as in for example QPSK, making it more resistant to fading where the constellation rotates because of the time-varying wireless channel. To make the technique easily implemented, it switches between two different sets of constellation points, as shown in Figure 2.5. From this Figure, we can see that the signal never passes through the origin, making it easier to implement in hardware than for example QPSK.

Let  $m(n)$  contain a sequence of values from the set  $[0, 1, 2, 3]$ , representing the symbols that we want to transmit: 00, 01, 11, and 10, respectively. The constellation points may then be calculated by the formula:

$$y(n) = y(n-1)e^{j\frac{\pi}{4} + j\pi m(n)/2} \quad (2.9)$$

From this formula we see that the phase difference between two consecutive data points,  $y(n)$  and  $y(n-1)$ , is given by the exponential factor  $e^{j\frac{\pi}{4} + j\pi m(n)/2}$  which may take the values  $\pi/4$ ,  $3\pi/4$ ,  $5\pi/4$  or  $7\pi/4$ . It is the  $\pi/4$ -term in the exponential that gives us the switching between two sets of constellation points, and it is the fact that  $y(n)$  depends on the old output,  $y(n-1)$ , that makes the information lie in the phase shifts rather than in the phase itself.

At the receiver, we only have to calculate the difference between the received phases and find the closest constellation point with phases  $\pi/4$ ,  $3\pi/4$ ,  $5\pi/4$ ,  $7\pi/4$ :

$$\begin{aligned}\angle y(n) - \angle y(n-1) &= \angle \frac{y(n)}{y(n-1)} = \\ &= \angle \frac{y(n-1)e^{j\frac{\pi}{4}+j\pi m(n)/2}}{y(n-1)} = \angle e^{j\frac{\pi}{4}+j\pi m(n)/2} = \\ &\frac{\pi}{4} + \pi m(n)/2 \in \{45^\circ, 135^\circ, 225^\circ, 315^\circ\}\end{aligned}\quad (2.10)$$

### Example

We want to transmit the sequence of bits

$$00 \ 01 \ 10 \ 11 \quad (2.11)$$

which corresponds to the sequence of constellation points  $m(n)$ , where Gray coding is used:

$$m(n) = [0, 1, 3, 2] \quad (2.12)$$

Let us calculate  $y(n)$  for each value of  $n$ :

$$\begin{aligned}y(0) &= y(-1)e^{j\frac{\pi}{4}+j\pi m(0)/2} = e^{j\frac{\pi}{4}} \\ y(1) &= y(0)e^{j\frac{\pi}{4}+j\pi m(1)/2} = e^{j\frac{\pi}{4}}e^{j\frac{\pi}{4}+j\pi/2} = e^{j\pi} \\ y(2) &= y(1)e^{j\frac{\pi}{4}+j\pi m(2)/2} = e^{j\pi}e^{j\frac{\pi}{4}+j3\pi/2} = e^{j3\pi/4} \\ y(3) &= y(2)e^{j\frac{\pi}{4}+j\pi m(3)/2} = e^{j3\pi/4}e^{j\frac{\pi}{4}+j\pi} = 1\end{aligned}\quad (2.13)$$

The sequence  $y(n)$  now contain the data that are to be interpolated (by **block 3**) and pulse shaped by the SRRC filter (**block 4**).

At the receiver, we apply (2.10) and get the values  $\frac{\pi}{4}$ ,  $\frac{3\pi}{4}$ ,  $\frac{7\pi}{4}$  and  $\frac{5\pi}{4}$  which corresponds to the same sequence  $m(n)$  as the one that was transmitted.

## 2.5 The square-root raised cosine filter (pulse shaping)

The impulse response of the SRRC filter is defined as [MCT]

$$h(t) = -4r \frac{\cos((1+r)\pi t/T_s) + \frac{\sin((1-r)\pi t/T_s)}{4rt/T_s}}{\pi\sqrt{T_s}((4rt/T_s)^2 - 1)} \quad (2.14)$$

where  $r$  is the rolloff factor,  $T_s$  is the symbol duration and  $t$  is time. The definition cannot be used in a straight forward manner when it is implemented since the second term of the nominator contains a division by  $t$  that might be zero. Also, the denominator of  $h(t)$  becomes zero when  $t = t/(4r)$ , since

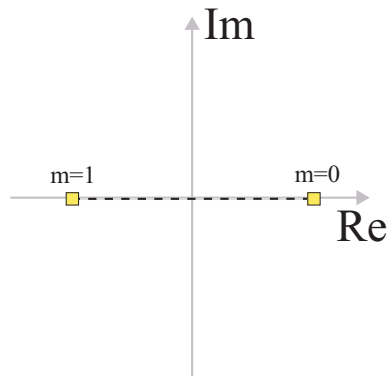


Figure 2.3: *Constellation diagram for BPSK: Transitions takes place between the two points where each one represents a bit.*

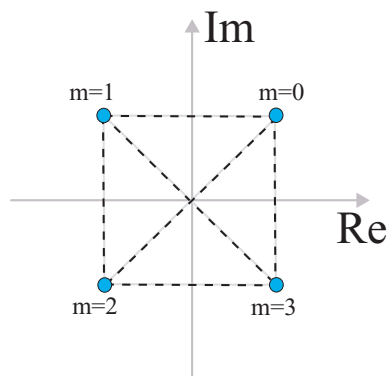


Figure 2.4: *Constellation diagram for QPSK: Transitions takes place between the four points where each one represents a symbol.*

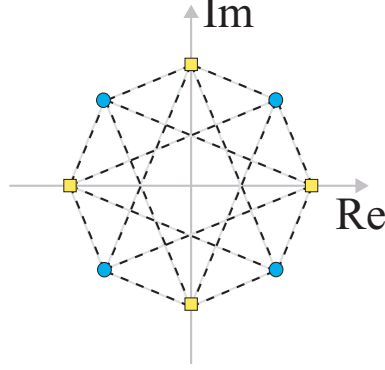


Figure 2.5: *Constellation diagram for  $\pi/4$ -DQPSK: Transitions takes place between one of the four points in the first subconstellation (circles) and any of the points in the next subconstellation (squares). The information is contained in the phase shifts rather than in the points themselves.*

$$\begin{aligned}
 \pi\sqrt{T_s}((4rt/T_s)^2 - 1) &= 0 \Leftrightarrow \\
 (4rt/T_s)^2 - 1 &= 0 \Leftrightarrow \\
 (4rt/T_s) &= 1 \Leftrightarrow \\
 t &= \frac{T_s}{4r}
 \end{aligned} \tag{2.15}$$

This implies that we have to find the values of  $h(t)$  when  $t \rightarrow 0$  and  $t \rightarrow \frac{T_s}{4r}$ , and treat these points as special cases in the implementation.

## 2.6 Channel model

The channel model or simulator is capable of simulating three types of channels: *time-invariant channels*, *flat fading channels* and *frequency selective fading channels*. In the first case, the channel impulse responses are defined before the simulation starts and does not change during the simulation. In the second case, the channel impulse responses contain a single coefficient that fades according to the Doppler frequency. Finally, in the third case, the responses contain several coefficients at fixed positions that fades according to the specified Doppler frequency. The simulator supports Rayleigh fading coefficients, where signals are supposed to reach the receiver antenna from all directions, as described on page 5.

### 2.6.1 Simulation of the fading channel coefficient

In the simulator the so called *modified sums of sinusoids version of Jakes method* [NH01] is implemented for simulation of a Rayleigh fading coefficient  $c(n)$  with a certain Doppler frequency. The parameters that have to be set are the carrier frequency  $f_c$ , the velocity of the mobile  $v$ , the sampling frequency  $F_s$  and a parameter  $K_0$  that controls the number of oscillators in the model. From these parameters, the maximum possible Doppler frequency shift  $f_{\max}$  can be calculated from

$$f_{\max} = \frac{v/\lambda}{F_s} \quad (2.16)$$

where  $\lambda$  is the wavelength of the carrier defined by

$$\lambda = \frac{v_{\text{light}}}{f_c} \quad (2.17)$$

where  $v_{\text{light}}$  is speed of light.

A fading coefficient can then be calculated as the sum of the in-phase and quadrature components,  $c_i(n)$  and  $c_q(n)$  respectively

$$c(n) = c_i(n) + \sqrt{-1}c_q(n) \quad (2.18)$$

The components are calculated via two formulas

$$c_i(n) = 2 \sum_{k=1}^{K_0} \left( \cos(\beta_k) \cos \left( 2\pi f_{\max} n \cos \left( \frac{2\pi k}{4K_0+2} \right) + \gamma_k \right) \right) + \sqrt{2} \cos(2\pi f_{\max} n + \gamma_{(K_0+1)}) \quad (2.19)$$

$$c_q(n) = 2 \sum_{k=1}^{K_0} \left( \sin(\beta_k) \cos \left( 2\pi f_{\max} n \cos \left( \frac{2\pi k}{4K_0+2} \right) + \gamma_k \right) \right) \quad (2.20)$$

Here, the variables  $\beta_k$  and  $\gamma_k$  stochastic variables uniformly distributed in  $[0, 2\pi]$ .

### 2.6.2 Construction of the discrete time impulse response

An impulse response of a baseband wireless channel consists in general of a number of impulses; each impulse has its own phase, amplitude and delay

because of different travel distances and attenuation of the wave it represents. Thus, the baseband impulse response can be represented as the sum of impulses defined by:

$$g(t) = \sum_{m=1}^M c_m(t) \delta(t - \tau_m) \quad (2.21)$$

where  $c_m(t)$  in general is a time-variant complex numbered coefficient and  $\tau_m$  is the delay of the  $m$  - th wave.

In order to simulate such an impulse response, we have to sample it first. Plain sampling of (2.21) by setting  $t = n/F_s$  is not practical since we would miss all impulses whose delay is not exactly a multiple of the sampling interval. One solution to this problem is to use an anti-aliasing filter before the sampler. In our simulator, we have chosen to filter  $g(t)$  with a brick wall filter with the cut-off frequency  $F_c < F_s/2$  which results in

$$g'(t) = \sum_{m=1}^M c_m(t) \cdot \frac{\sin(2\pi F_c \cdot (t - \tau_m))}{\pi \cdot (t - \tau_m)} \quad (2.22)$$

The impulse response in (2.22) can be sampled by setting  $t = n/F_s$ .

### 2.6.3 The spatial-temporal channel model

When an antenna array is used at the receiver it is possible to use beam-forming algorithms to form a lobe in direction of the desired signal and place nulls in the directions of unwanted signals. A channel model which takes this spatial information into account is called a *spatial-temporal* channel model in contrast to the *temporal* model we have considered so far.

A common assumption in the simulation of spatial-temporal channels is that the signal received at each antenna element will be the same with the exception of a phase shift that depends on the angle of arrivals and the geometry of the antenna array [LR99]. The difference in phase between the received signal at the antenna in the origin and the antenna positioned at the coordinate  $(x_k, y_k, z_k)$  is:

$$\Delta\theta(p, k) = \beta x_k \cos \phi_p \sin \varphi_p + \beta y_k \sin \phi_p \cos \varphi_p + \beta z_k \cos \varphi_p \quad (2.23)$$

where  $\beta = 2\pi/\lambda$  is the phase propagation factor,  $\lambda$  the wavelength of the carrier and  $(\phi_p, \varphi_p)$  the direction of arrival for the signal. The expression in (2.23) may be simplified when the elevation angle  $\varphi_p$  represent the horizon ( $\varphi_p = 90^\circ$ ) and we consider an array with all elements distributed with equal

distance  $\Delta x$  on the x-axis (i.e.,  $y_m = z_m = 0$ ), as in the case of linear equally spaced (LES) array. Under these assumptions, (2.23) can be re-written as

$$\Delta\theta(p, k) = \beta k \Delta x \cos \phi_p \quad (2.24)$$

The simulator is capable of taking the angle of arrival of each wave reaching the antenna array into account and adjusting the phases accordingly.

There are also models available which include the possibility to control the amount of correlation between antenna elements, see for example [ER98], but these are not yet supported in our simulator.

# Chapter 3

## Computer experiments

In this Chapter, we evaluate and verify the simulator for different cases: AWGN channels, time-invariant channels, and time-varying frequency selective fading channels. We also evaluate the performance of an equalizer and a beamformer, both adapted by RLS, for multipath fading channels.

### 3.1 Design of the discrete time impulse responses

The objective of this experiment is to verify the method for designing the discrete time impulse response from the baseband continuous time impulse response as described in Section 2.6.2. We verify the method by comparing the magnitude, phase and group delay of the designed discrete time impulse response to that of the continuous time impulse response. In order to do that, we derive the phase and group delay of the continuous time response.

The impulse response of a complex continuous time filter with two coefficients can be written as

$$h_2(t) = \alpha_1 e^{j\theta_1} \delta(t - \tau_1) + \alpha_2 e^{j\theta_2} \delta(t - \tau_2) \quad (3.1)$$

where  $\alpha_1$  and  $\alpha_2$  are (real valued) amplitudes,  $\theta_1$  and  $\theta_2$  phases and  $\tau_1$  and  $\tau_2$  delays of the two waves. The Fourier transform of (3.1) is given by

$$\begin{aligned} H_2(\Omega) &= \alpha_1 e^{j\theta_1} e^{-j\Omega\tau_1} + \alpha_2 e^{j\theta_2} e^{-j\Omega\tau_2} \\ &= e^{j(\theta_1 - \Omega\tau_1)} (\alpha_1 + \alpha_2 e^{-j(\Omega\tau_2 - \Omega\tau_1 + \theta_1 - \theta_2)}) \\ &= e^{j(\theta_1 - \Omega\tau_1)} H_1(\Omega) \end{aligned} \quad (3.2)$$

where  $H_1(\Omega)$  is the Fourier transform

$$H_1(\Omega) = \alpha_1 + \alpha_2 e^{-j\Gamma} \quad (3.3)$$

with

$$\Gamma = \Omega\tau_2 - \Omega\tau_1 + \theta_1 - \theta_2 \quad (3.4)$$

Using the laws of sinus and cosines, we can derive the phase of  $H_1(\Omega)$  as

$$\angle H_1(\Omega) = \begin{cases} -\sin^{-1} \left( \frac{\alpha_2 \sin(\pi-\Gamma)}{\sqrt{\alpha_1^2 + \alpha_2^2 - 2\alpha_1\alpha_2 \cos(\pi-\Gamma)}} \right) & , \operatorname{Re} \{H_1(\Omega)\} \geq 0 \\ -\pi - \sin^{-1} \left( \frac{\alpha_2 \sin(\pi-\Gamma)}{\sqrt{\alpha_1^2 + \alpha_2^2 - 2\alpha_1\alpha_2 \cos(\pi-\Gamma)}} \right) & , \operatorname{Re} \{H_1(\Omega)\} < 0 \end{cases} \quad (3.5)$$

This result can be used to calculate the phase of  $H_2(\Omega)$  by realizing, from (3.2), that

$$\angle H_2(\Omega) = \angle H_1(\Omega) + \theta_1 - \Omega\tau_1 \quad (3.6)$$

Using (3.2) the group delay can be derived and is given by

$$\tau_g = -\frac{d\angle H_2(\Omega)}{d\Omega} \quad (3.7)$$

The result is complicated, consisting of many terms and products, so we will not present it here.

As an example, consider the continuous time impulse response

$$h(t) = (-0.3 + 0.8i) \delta(t - 1/F_s) + (0.2 + 0.3i) \delta(t - 2.3/F_s) \quad (3.8)$$

In Figure 3.1 we show the amplitude spectrum, phase spectrum and group delay for the *continuous* and *discrete* (designed) time complex impulse responses respectively, together with the coefficients of the designed response. We used the sampling frequency  $F_s = 315900$  Hz and a cut-off frequency for the brick-wall filter of  $F_c = 0.5F_s$  Hz. The length of the designed filter was set to 16 coefficients. We can see from this Figure that the designed impulse response is in good agreement with desired characteristics of the original continuous response.

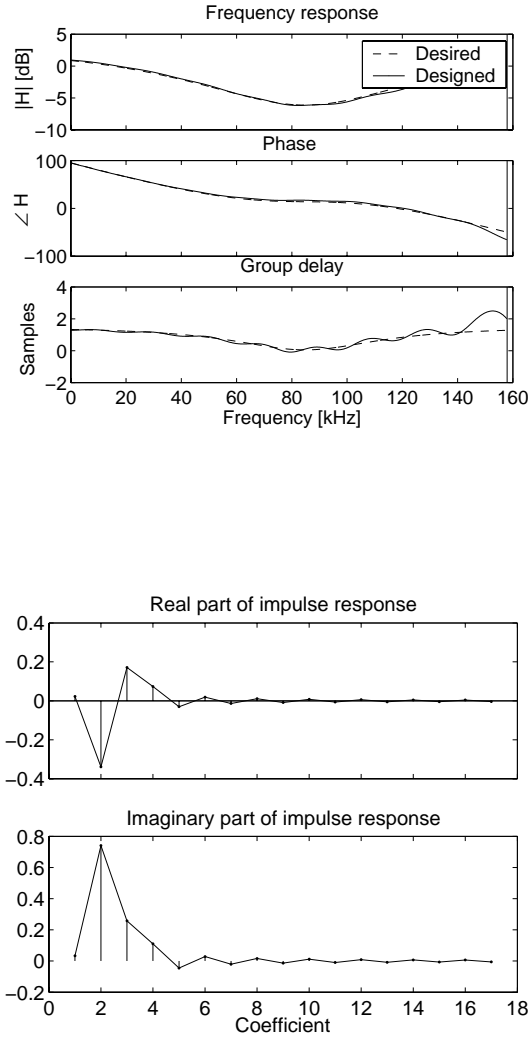


Figure 3.1: *Example of design of impulse response. The parameters used are: Sampling frequency  $F_s = 315900$  Hz, cut-off frequency for the brick-wall filter  $F_c = 0.5F_s$  Hz, length of filter 16 coefficients, impulses positioned at  $\tau_1 = 1/F_s$  and  $\tau_2 = 2.3/F_s$  seconds, and complex amplitudes  $0.8i-0.3$  and  $0.3i + 0.2$ .*

## 3.2 Simulation of a system with AWGN

In this Section we consider a system with a channel that is subject to additive white Gaussian noise (AWGN) only, and verify our simulation results by comparing them with the theoretical result of the chosen modulation scheme.

We use a setting where we transmit 10000 symbols in each of the 10 Monte Carlo simulation runs at the rate 24300 symbols/second. We use  $\pi/4$ -DQPSK modulation. In Figure 3.2 we show the bit error rate (BER) curves for no over sampling (or over sampling factor of 1), and in Figure 3.3 for an over sampling factor of 13. In the latter case, SRRC-filtering was also employed. It is evident from these Figures that the simulated and analytical BER are in good agreement. Consequently, we concluded that the simulator, *with a high-degree of confidence*, is correctly implemented.

## 3.3 Simulation of a time-invariant channel

In [YB00] BER curves are presented for different channels and equalizer structures. For example, they estimated the BER as a function of  $E_b/N_0$  for a channel with the impulse response

$$h(t) = 1.2\delta(t) + 1.1\delta(t - T_s) - 0.2\delta(t - 2T_s) \quad (3.9)$$

where  $T_s$  is the symbol duration. We refer to this channel as the "Yeh-Barry"-channel in Figures 3.4 to 3.6. In these Figures we also show the results from our simulator using the same channel and compare them to those obtained from [YB00] for the following cases: no over sampling, over sampling without SRRC and over sampling with SRRC, respectively. We use a setting where we transmit 10000 BPSK symbols in each of the 10 Monte Carlo runs. The symbol rate is 24300 symbols/second. The optimal equalizer (minimized MSE) was derived and used in all three cases. We can conclude from Figures 3.4 to 3.6 that the results from our simulator are in good agreement with the expected results, with exception for the case of SRRC-filtering where our simulator predicts better performance.

## 3.4 Simulation of a Rayleigh fading channel

We generated two realizations of a Rayleigh fading channel coefficient in order to verify that our implementation of Jakes method is correct. The verification was performed by calculating the statistics of the generated signal

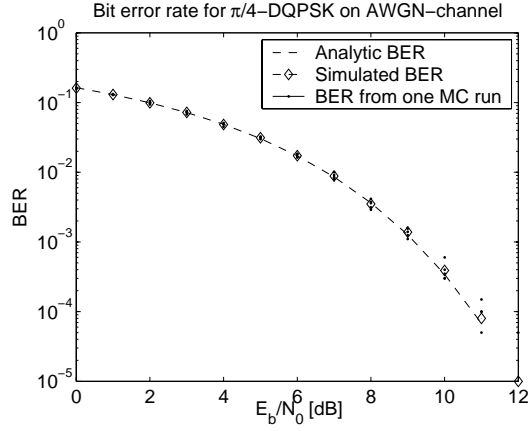


Figure 3.2: *Bit error rate as a function of  $E_b/N_0$ : AWGN-channel, over sampling factor = 1 samples/symbol and no SSRC-filter. Other parameters:  $10 \cdot 10000$  symbols, 24300 symbols/s,  $\pi/4$ -DQSPK and no equalizer used.*

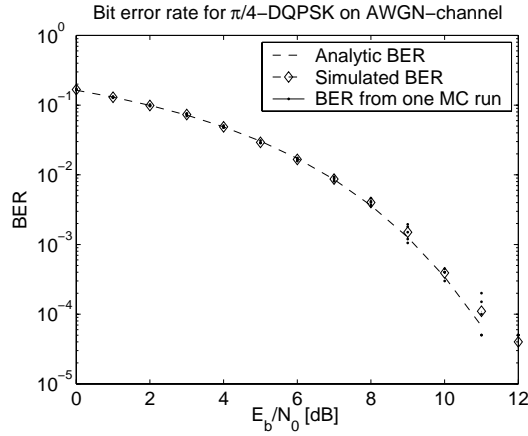


Figure 3.3: *Bit error rate as a function of  $E_b/N_0$ : AWGN-channel, over sampling factor = 13 samples/symbol and SSRC-filter is used. Other parameters as in Figure 3.2.*

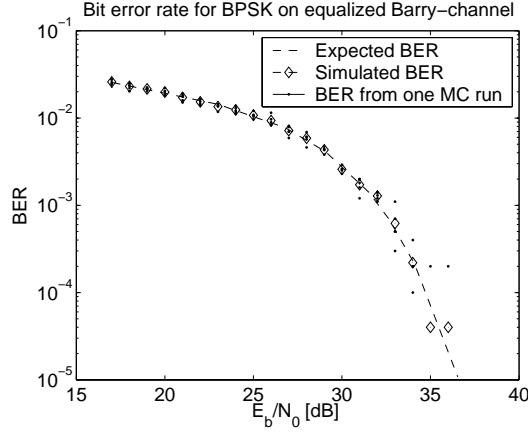


Figure 3.4: *BER as a function of  $E_b/N_0$ : "Yeh-Barry"-channel, no SSRC-filter,  $10 \cdot 10000$  symbols,  $24300$  symbols/s, BPSK, no over sampling,  $3 \cdot 1$  equalizer weights, delay =  $2 \cdot 1$  samples, optimal linear equalizer used.*

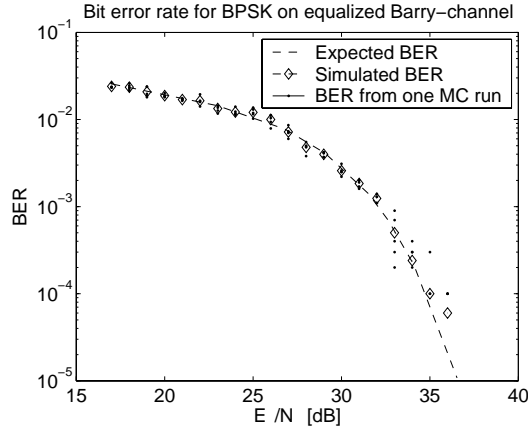


Figure 3.5: *BER as a function of  $E_b/N_0$ : "Yeh-Barry"-channel, no SSRC-filter,  $10 \cdot 10000$  symbols,  $24300$  symbols/s, BPSK, over sampling factor =  $13$  samples/symbol,  $3 \cdot 13$  equalizer weights, delay =  $2 \cdot 13$  samples, optimal linear equalizer used.*

and comparing them to the expected analytical statistics in the same manner as in [NH01].

In Figures 3.7 to 3.9 we show the eye diagrams of the magnitude of generated channel coefficients for 3, 50 and 200 km/h, respectively. The time duration on the x-axis corresponds to one slot of 162 symbols. We see that the higher the velocity, the faster the signal fades, as expected.

In Figures 3.10 to 3.14 the estimated probability density function (PDF), level crossing rate (LCR), amplitude fade duration (AFD), power spectral density (PSD) and autocorrelation is shown together with the expected analytical curves for a normalized Doppler frequency of 0.01. From these Figures we can see good agreement between the results of the simulated and analytical statistics. The crosscorrelation between the two independently generated fading coefficients in Figure 3.15 also shows that they are uncorrelated as required.

Finally, to verify that the complete system with modulation, SRRC-filters, channel and demodulation works as expected, we simulated and plotted the BER for varying  $E_b/N_0$  as shown in Figure 3.16. The analytical BER for a Rayleigh fading channel is calculated according to [Pro95], equation (14-3-7) on page 774:

$$P_e = \frac{1}{2} \left( 1 - \sqrt{\frac{E_b/N_0}{1 + E_b/N_0}} \right)$$

In the figure, we can see good agreement between the analytical and simulated BER results.

### 3.5 Simulation of a frequency selective fading channel

In [FRT93] simulation results and references to analytical results for frequency selective multipath channels consisting of two Rayleigh fading coefficients with different delays are presented. In Figure 3.17 we compare the results from our simulator to the expected analytical BER, using the same configuration used in this article.

Figure 3.17 shows BER versus C/D, which is defined as the average power ratio of the first wave to the second wave in the two-wave Rayleigh fading channel. The delayed wave arrives seven samples later than the first wave and the carrier to interference ratio (C/I) was set to infinity (i.e. no interference) and  $E_b/N_0$  to 100 dB. The rest of the parameters are given in the caption to

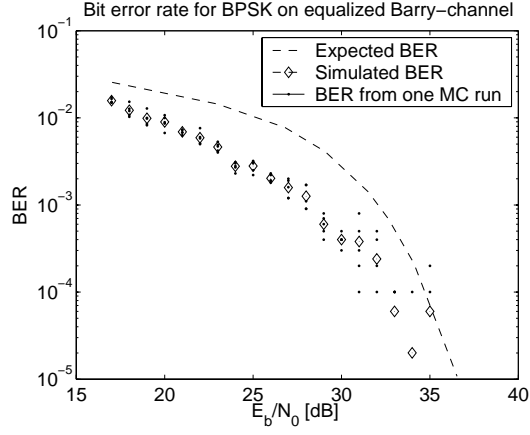


Figure 3.6: *BER as a function of  $E_b/N_0$ : "Yeh-Barry"-channel, SSRC-filter is used, and other parameters as in Figure 3.5.*

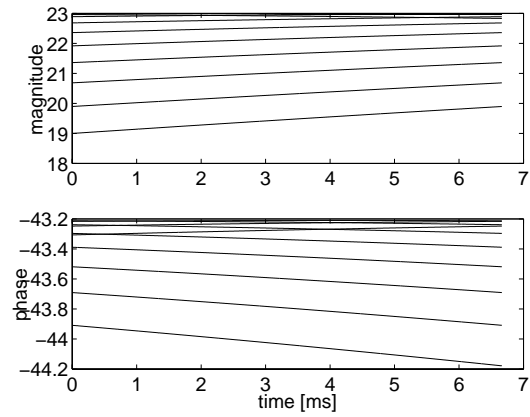


Figure 3.7: *Eye diagram for a Rayleigh fading signal for a velocity of 3 km/h.*

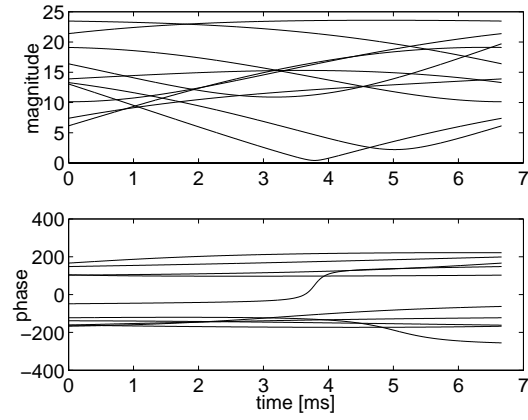


Figure 3.8: *Eye diagram for a Rayleigh fading signal for a velocity of 50 km/h.*

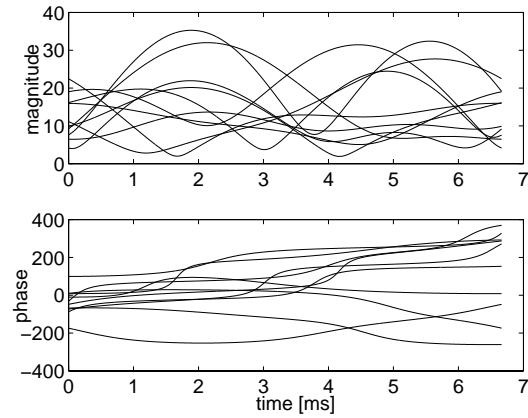


Figure 3.9: *Eye diagram for a Rayleigh fading signal for a velocity of 200 km/h.*

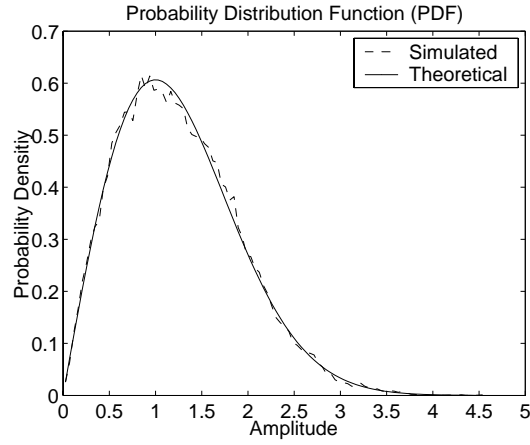


Figure 3.10: *Estimated and analytical probability density function (PDF) for a Rayleigh fading channel with a normalized doppler frequency of  $f_n = 0.01$ .*

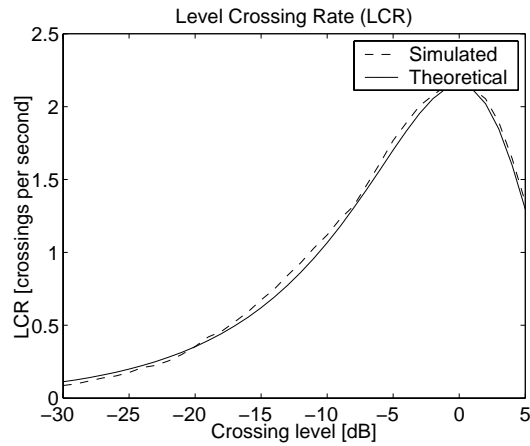


Figure 3.11: *Estimated and analytical level crossing rate (LCR) for a Rayleigh fading channel with a normalized doppler frequency of  $f_n = 0.01$ .*

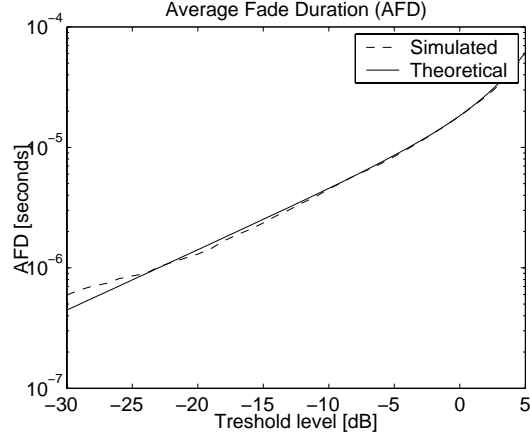


Figure 3.12: *Estimated and analytical amplitude fade duration (AFD) for a Rayleigh fading channel with a normalized Doppler frequency of  $f_n = 0.01$ .*

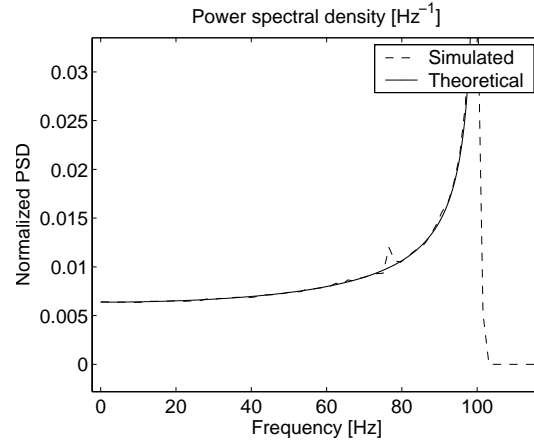


Figure 3.13: *Estimated and analytical power spectral density (PSD) for a Rayleigh fading channel with a normalized Doppler frequency of  $f_n = 0.01$ .*

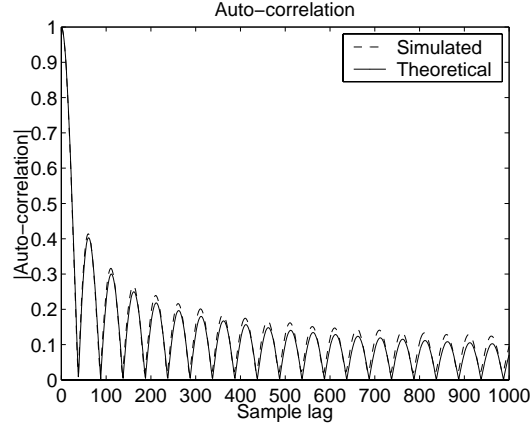


Figure 3.14: *Estimated and analytical autocorrelation for a Rayleigh fading channel with a normalized doppler frequency of  $f_n = 0.01$ .*

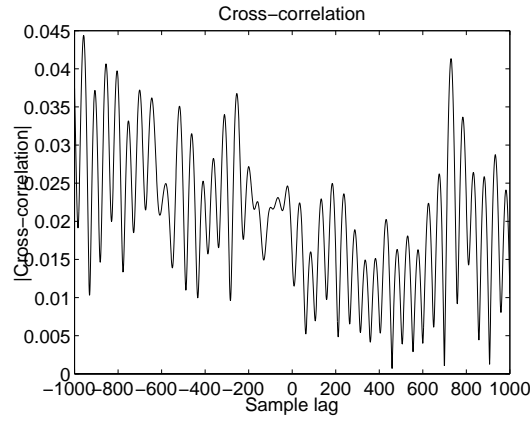


Figure 3.15: *Estimated crosscorrelation between two Rayleigh fading coefficients with a normalized doppler frequency of  $f_n = 0.01$ .*

the Figure. Again, we can see that the simulated and analytical results are in good agreement.

### 3.6 Simulation of a RLS equalizer for a frequency selective fading channel

We simulate a system with an equalizer in order to estimate its performance and to have a benchmark which we can use when developing new equalizer structures. In this experiment, we choose to simulate the exponentially weighted recursive least squares (RLS) based equalizer [Hay02].

The RLS equalizer is initialized with a forgetting factor of 0.999 and regularization parameter  $10^{-7}$ . The channel consists of three paths with delays of 0,  $0.5T_s$  and  $T_s$  seconds respectively. The channel impulse response is modelled by using 13 samples, and the over sampling factor is 13. We use  $E_b/N_0 = 10$  dB and simulate the equalizer for different settings of the delay of the desired signal and number of coefficients. The carrier frequency is 850 MHz and the symbol rate 24300 symbols/second. The modulation technique used was  $\pi/4$ -DQPSK.

In Figure 3.18 we show BER as a function of velocity for a system where RLS is active during the whole slots, using all data as a training sequence. This corresponds to the case of a RLS equalizer using decision feedback with no decision errors in the feedback. In Figure 3.19, on the other hand, the RLS equalizer is only active during the training sequence in the beginning of each slot. We report the following observations:

- For low velocities, the RLS equalizer improves performance, especially when using longer filter and longer multipath delay.
- The RLS equalizer does not provide improved performance if the velocity is too high.
- For the case of continuous mode in Figure 3.18, the RLS equalizer is useful for velocities approximately below 70 km/h.
- For the case of slotted mode in Figure 3.19, the RLS equalizer is useful for velocities approximately below 30 km/h.

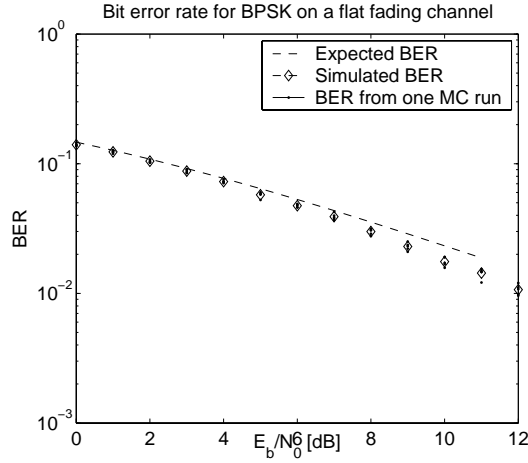


Figure 3.16: *Bit error rate versus signal to noise ratio for BPSK in a Rayleigh fading channel. Settings: 850 MHz, 24300 symbols/s, SRRC with rolloff factor 0.2, normalized doppler frequency  $f_n = 0.01$ ,  $1 \cdot 10000$  symbols, over sampling factor = 13 samples/symbol, no equalizer used.*

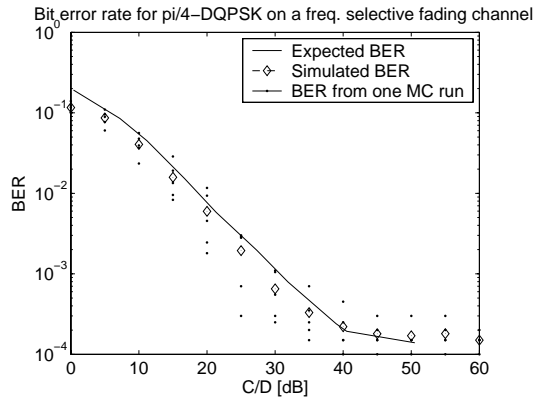


Figure 3.17: *BER versus C/D for  $\pi/4$ -DQPSK in a frequency-selective two-wave Rayleigh fading channel for a seven sample signal delay.  $E_b/N_0 = 100$  dB, 850 MHz, 24300 symbols/second, velocity 120 km/h, SRRC-filter with roll-off factor 0.2,  $10 \cdot 10000$  symbols,  $\pi/4$ -DQPSK, over sampling factor = 13 samples/symbol, no equalizer used.*

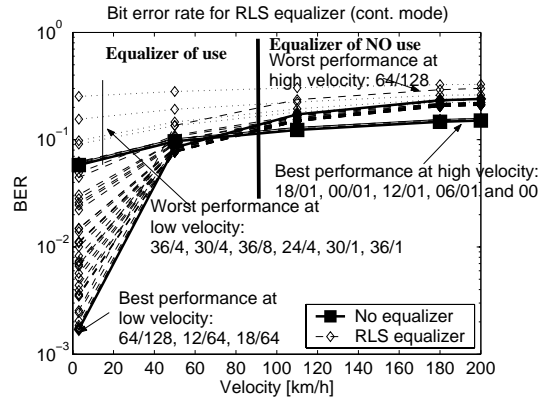


Figure 3.18: *BER as a function of velocity for the RLS equalizer in a continuous mode system with different delays and coefficients (denoted  $x/y$  where  $x$  is the delay and  $y$  the number of coefficients) in comparison with the case of no equalizer at all.*

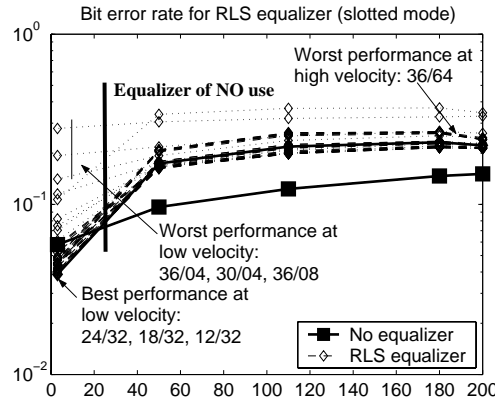


Figure 3.19: *BER as a function of velocity for the RLS equalizer in a slotted mode system with different delays and coefficients (denoted  $x/y$  where  $x$  is the delay and  $y$  the number of coefficients) in comparison with the case of no equalizer at all.*

### 3.7 Simulation of a RLS beamformer for a frequency selective fading channel

We have simulated a RLS beamformer in order to evaluate its performance for a spatial-temporal channel. The settings used are: 7 interfering users, 8 antenna elements in a circular configuration with a spacing of half a wavelength, 8 coefficients in the beamformer, modulation technique  $\pi/4$ -DQPSK,  $E_b/N_0 = 10$  dB, delay zero. Each one of the 8 users (the desired user and the seven interferers) experiences a three coefficient channel, where each coefficient is Rayleigh fading and with delays 0,  $0.5T_s$  and  $T_s$  seconds. The angle of arrivals (in degrees) for the desired user ( $p = 1$ ) and the interferers are given in the table below:

coefficient	p=1	p=2	p=3	p=4	p=5	p=6	p=7	p=8
1	0	55	80	140	182	221	265	323
2	4	59	79	144	178	220	268	318
3	-4	52	77	141	180	218	260	325

In Figure 3.20 we show the BER for different velocities. We see that the use of a beamformer improves the performance for all velocities in comparison to the case of using no beamformer at all.

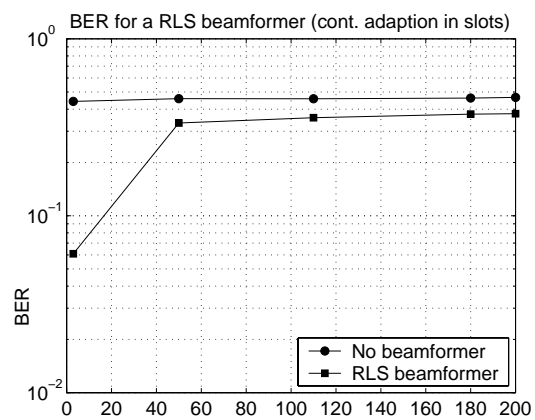


Figure 3.20: *BER as a function of velocity for the RLS beamformer in a continuous mode system in comparison with the case of no beamformer at all.*

# Chapter 4

## Conclusions

In this Report the basic propagation factors (path loss, large-scale and small-scale fading) which degrade the quality and performance of wireless communication systems were presented. We also presented and implemented a simulator for assessing the performance of wireless fading channels. In addition, we presented some useful statistical properties for these channels; these included the probability density function (PDF), level crossing rate (LCR), amplitude fade duration (AFD), power spectral density (PSD), and the autocorrelation and crosscorrelation functions. Further more, we evaluated and verified the simulator for different cases: AWGN channels, time-invariant channels, and time-varying frequency selective fading channels. We also presented basic equalization and beamforming concepts, and evaluated the performance of RLS based equalizer and beamformer receiver structures (using the simulator) for multipath fading channels. These receiver structures are effective means in combating the destructive effects of intersymbol and cochannel interference in these channels, thereby improving the signal quality and performance of wireless communication networks.

# Bibliography

- [CHLP94] J.D. Crockett, E.D. Hoole, T. Labno, and S. Popik. IS-54 simulation - application report. Technical report, Texas Instruments, 1994.
- [Chr02] M. Chrysomallis. Simulation of mobile fading channels. *IEEE Antennas and Propagation Magazine*, 44(6):172–183, 2002.
- [Cla68] R. H. Clarke. A statistical theory of mobile-radio reception. *Bell Syst. Tech. Journal*, 47:957–1000, July/Aug 1968.
- [DHFM02] A. Duel-Hallen, T.L Fulghum, and K.J Molnar. The jakes fading model for antenna arrays incorporating azimuth spread. *IEEE Transactions on Vehicular Technology*, 51(5):968–977, September 2002.
- [ECS<sup>+</sup>98] R.B. Ertel, P. Cardieri, K.W. Sowerby, T.S. Rappaport, and J.H. Reed. Overview of spatial channel models for antenna array communication systems. *IEEE Personal Communications*, 5(1):10–22, Feb 1998.
- [ER98] R.B. Ertel and J.H. Reed. Generation of two equal power correlated rayleigh fading envelopes. *IEEE Communications Letters*, 2(10):276–278, Oct 1998.
- [FRT93] Victor Fung, Theodore S. Rappaport, and Berthold Thoma. Bit error simulation for  $\pi/4$ -DQPSK mobile radio communications using two-ray and measurement-based impulse response models. *IEEE Journal on Selected Areas in Communications*, 11(3):393–405, April 1993.
- [Hay02] S. Haykin. *Adaptive Filter Theory*. Prentice Hall, 4th edition, 2002.

- [Hoo94] E.D. Hoole. Channel equalization for the IS-54 digital cellular system with the tms320c5x - application report. Technical report, Texas Instruments, 1994.
- [Jak94] W.C. Jakes. *Microwave Mobile Communication*. IEEE Press, New Jersey, 1994.
- [LR99] J.C. Liberti and T. S. Rappaport. *Smart Antennas for Wireless Communications - IS-95 and Third Generation CDMA Applications*. Prentice Hall, 1999.
- [MCT] *Matlab Communications Toolbox*.
- [NH01] J. Nordberg and Hai Huyen dam. Evaluation of different rayleigh fading channel simulators. Technical report, ATRI, Curtin University, Australia, 2001.
- [Pro95] J.G. Proakis. *Digital Communications*. Electrical and Computer Engineering. McGraw-Hill, 3rd edition, 1995.
- [Pt02] M. Ptzold. *Mobile Fading Channels*. Wiley, 2002.
- [Sma94] D. Smalley. Equalization concepts - a tutorial (application report). Technical report, Texas Instruments, 1994.
- [Sta02] W. Stallings. *Wireless Communications and Networks*. Prentice-Hall, New Jersey, 2002.
- [Tid99] C. Tidestav. *The Multivariable Decision Feedback Equalizer - Multiuser Detection and Interference Rejection*. PhD thesis, Uppsala University, 1999.
- [YB00] Chen-Chu Yeh and John R. Barry. Adaptive minimum bit-error rate equalization for binary signaling. *IEEE Transactions on Communications*, 48(7):1226–1235, July 2000.



Simulation of Wireless Fading Channels  
Ronnie Gustafsson & Abbas Mohammed

ISSN 1103-1581  
ISRN BTH-RES--02/03--SE

Copyright © 2003 by the authors  
All rights reserved  
Printed by Kaserntryckeriet AB, Karlskrona 2003